Global and Planetary Change 143 (2016) 81–87

Contents lists available at ScienceDirect

Global and Planetary Change

journal homepage: www.elsevier.com/locate/gloplacha

Recent glacier changes in the Tien Shan observed by satellite gravity measurements

Shuanggen Jin [a,*], X. Tian[a,b], G. Feng [a]

[a] Shanghai Astronomical Observatory, Chinese Academy of Sciences, Shanghai 200030, China
[b] University of Chinese Academy of Sciences, Beijing 100049, China

ARTICLE INFO

Article history:
Received 10 September 2015
Received in revised form 13 November 2015
Accepted 10 June 2016
Available online 11 June 2016

Keywords:
Glacier melting
Tien Shan
GRACE
WGHM

ABSTRACT

The glaciers in the Tien Shan are extensive and play an important role in water cycle in central Asia. However, it is difficult to accurately monitor glacier variations in the Tien Shan due to the lack of in situ widespread measurements. In this paper, glacier mass variations in the Tian Shan are obtained and investigated from 10 years of monthly GRACE gravity solutions (January 2003–December 2012) and the WaterGAP Global Hydrology Model (WGHM), including seasonal, secular and interannual variations. Results show that significant seasonal variations of glacier mass are found with the maximum normally in April–June and the minimum around in November–December. The trends in all four regions are positive from 2002 to 2005 and negative from 2005 to 2012, indicating that the Tien Shan glaciers are increasing prior to 2005 and significantly melting after 2005. These changes are consistent with the temperature change in the Tien Shan. In addition, in the past decade the precipitation has decreased and evapotranspiration has increased, which have joint influences on glacier mass changes in different regions of the Tien Shan.

1. Introduction

The Tien Shan is located in central Asia, through central Xinjiang Province, China with the western end stretching into Kazakhstan. The total glacier area in the Tien Shan is ~10,100 km^2. Fig. 1 shows the distribution of glaciers in the Tian Shan. The World Glacier Inventory (WGI) (http://nsidc.org/data/glacier_inventory/browse.html) contains information for over 130,000 glaciers in the Tien Shan, including geographic location, area, length, orientation, elevation and classification. However, the Tien Shan has a mean elevation of over 3000 m, and it is thus very difficult to accurately monitor glacier variations due to the lack of in situ widespread measurements (e.g. evapotranspiration, precipitation, surface run-off and soil moisture).

Earth's continental ice sheets are changing, related to the temperature, precipitation, river runoff and evapotranspiration, which affect and are affected by changes in Earth's climate (Jin et al., 2013). Due to recent global warming, some glaciers are melting and cause sea level rise (e.g., Avsar et al., 2016). Glacier shrinkage in the Tien Shan has recently been reported based on remote sensing data (e.g. Aizen et al., 2006; Niederer et al., 2008; Narama et al., 2006; Jing et al., 2006; Li et al., 2006; Shangguan et al., 2006; Liu et al., 2006). However, remote sensing data have some limitations, such as low temporal resolution and limited study area. Furthermore, various types of remotely sensed data with different time periods make them difficult to compare. The recent development of satellite gravimetric techniques has given us a new opportunity to measure glacier mass change (e.g. Jin et al., 2013, 2014). The Gravity Recovery and Climate Experiment (GRACE) mission, launched in 2002, has been very successful to monitore the Earth's time-variable gravity field by determining accurately the relative position of a pair of Low Earth Orbit (LEO) satellites. GRACE satellite gravimetry offers the unique opportunity to directly measure mass redistribution by monitoring gravity change, which has been widely used, such as ice sheet mass balance, terrestrial water storage (TWS), sea level rise, and ocean circulation (e.g. Velicogna and Wahr, 2005; Velicogna, 2009; Frappart et al., 2008; Rodell et al., 2009; Morison et al., 2007; Jin et al., 2010, 2011; Hassan and Jin, 2016). Over the land, the detailed monthly gravity field solutions can estimate TWS variations (Wahr et al., 1998; Jin et al., 2012; Jin and Feng, 2013; Shen et al., 2015). After excluding the surface water, snow, canopy water and groundwater, the ice sheets storage variations can be estimated.

In this paper, the total water storage variation with monthly resolution is derived from 10 years of monthly GRACE measurements (2003 January–2012 December), and ice mass variations in the Tien Shan are obtained by subtracting the surface water, snow, canopy water and groundwater from the hydrological model, WGHM (WaterGAP Global Hydrology Model). The seasonal ice mass variations and trends in the Tian Shan are investigated from ~10 years of monthly ice mass variation time series.

* Corresponding author at: Shanghai Astronomical Observatory, Chinese Academy of Sciences, Shanghai 200030, China.
E-mail addresses: sgjin@shao.ac.cn, sg.jin@yahoo.com (S. Jin).

http://dx.doi.org/10.1016/j.gloplacha.2016.06.006
0921-8181/

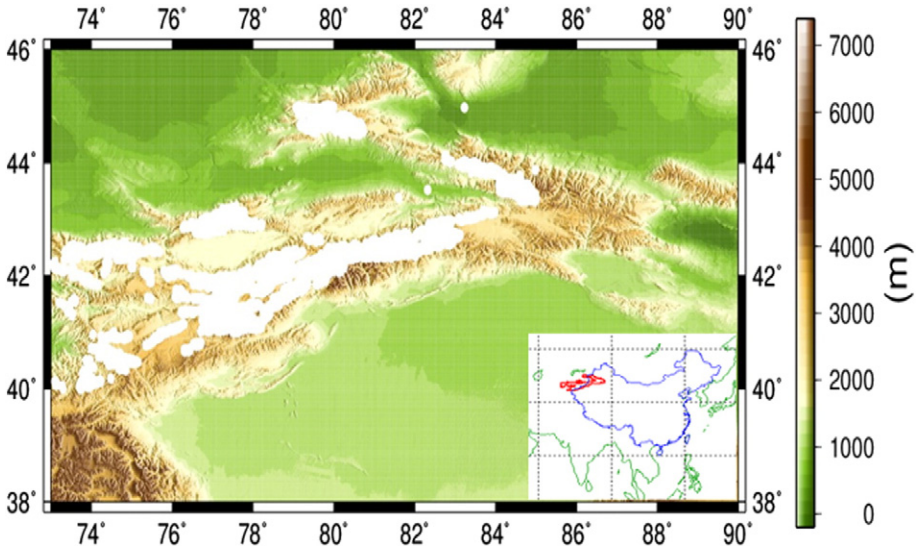

Fig. 1. Distribution of glaciers in the Tien Shan and surroundings.

2. Observations and methods

2.1. Terrestrial water storage from GRACE

The GRACE Project delivers sets of spherical harmonic coefficients describing the temporal Earth's gravity field variations, which can be used to study the Earth's mass redistribution caused by, for example, fluctuations in terrestrial water storage, changes in the polar ice sheets and changes in atmospheric and oceanic mass (Wahr et al., 1998). After atmospheric and oceanic mass effects are removed from climate and ocean circulation models, the remaining signals are mostly related to variations of TWS (Zhao et al., 2015). TWS anomalies over the land, $\Delta\eta_{\text{land}}$ can thus be directly described by gravity coefficient anomalies (ΔC_{lm}, ΔS_{lm}) (Swenson and Wahr, 2002):

$$\Delta\eta_{\text{land}}(\theta,\phi,t) = \frac{a\rho_{\text{ave}}}{3\rho_{\text{w}}}\sum_{l=0}^{\infty}\sum_{m=0}^{l}\tilde{P}_{lm}(\cos\theta)\frac{2l+1}{1+k_l}(\Delta C_{lm}\cos(m\phi)+\Delta S_{lm}\sin(m\phi)) \quad (1)$$

where ρ_{ave} is the average density of the Earth, ρ_{w} is the density of fresh water, a is the equatorial radius of the Earth, $\tilde{P}_{lm}$ is the fully-normalized associated Legendre function of degree l and order m, k_l is Love number of degree l (Han and Wahr, 1995), θ is the spherical co-latitude, ϕ is the longitude and t is the time. Due to measurement errors and noise in the GRACE data, we have used the post-process and applied for a factor to the GRACE data after filtering following Landerer and Swenson (2012): degree 2, order 0 coefficients are taken from satellite laser ranging (Cheng and Tapley, 2004), degree 1 coefficients are replaced from Swenson et al. (2008), a de-striping filter and a 500 km Gaussian spatial smoother are applied (Swenson and Wahr, 2006; Jekeli, 1981) and post-glacial rebound signals are removed according to the model of Paulson et al. (2007) as revised by Geruo et al. (2013). Monthly TWS anomalies are calculated based on GRACE Release 5 (RL05) gravity field data from January 2003 to December 2012 (excluding June 2003, January 2011, June 2011, May 2012 and October 2012 with missing data), provided by the Center for Space Research (CSR) at the University of Texas, Austin (Bettadpur, 2007).

2.2. Land water storage from WGHM model

The WaterGAP Global Hydrological Model (WGHM) (Döll et al., 2003; Güntner et al., 2007) was developed to analyze water resources and water use in river basins, with a resolution of 0.5° × 0.5°. The model computes monthly time-series of surface and subsurface runoff, groundwater recharge and river discharge as well as storage variations of water in canopy, snow, soil, groundwater, lakes, wetlands and rivers. Therefore, the total continental water storage described in the model is the sum of canopy, snow, soil and groundwater storage as well as water stored in surface water bodies, e.g. rivers, wetlands, lakes and reservoirs. Here, we calculate the land water storage, including snow water storage, soil moisture storage, surface water storage and groundwater storage, based on the latest WGHM model's components with 1° spatial resolution from January 2003 to December 2012. In order to be consistent with GRACE results, we firstly use an interpolation method to adjust the spatial resolution from 0.5° to 1° and then use the same Gaussian filter and de-striping filter to process spherical harmonic coefficients from the WGHM model to eliminate errors in the data processing. Thus, the land water storages are obtained based on the processed spherical harmonic coefficients. To mitigate the leakage errors of signals, we convert water storage from WGHM to gravity coefficients for a unit amplitude mass signal over the glaciers in each region using the destriping filter and Gaussian smoothing, which are compared with the unit amplitude mass signal, and we can obtain the scaling factors with about 1.1 for the GRACE estimates.

2.3. Ice mass storage

The TWS estimated from GRACE includes groundwater, snow, glaciers, soil moisture, surface water and biological water. The land water storage from the WGHM model contains groundwater, snow, soil moisture, surface water and biological water, without the ice masses. After subtracting the WGHM land water storage from total continental water storage determined by GRACE, the monthly ice-mass storage changes are obtained in the Tien Shan for the available months.

3. Results and analysis

The ice mass storage variability has strong seasonal and secular signals. We therefore use a model including the annual, semi-annual and linear trend terms to fit the ice mass variation time series as (Jin and Feng, 2013):

$$M(t) = a + bt + \sum_{k=1}^{2} c_k\cos(\omega_k t - \phi_k) + \varepsilon(t) \quad (2)$$

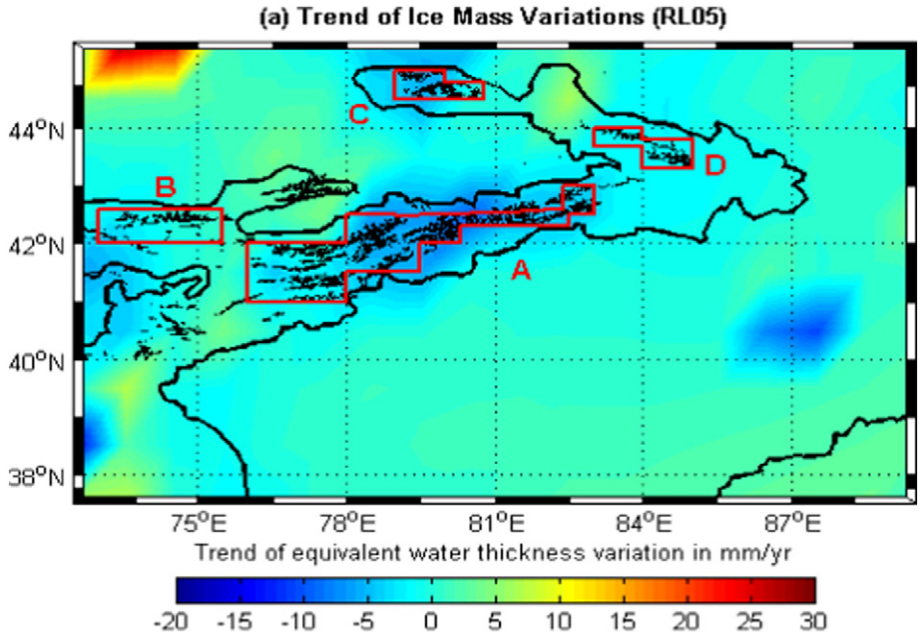

Fig. 2. The trend of ice mass variability in the Tien Shan and surroundings.

where $M(t)$ is the ice mass, t is the time, a is the constant, b is the trend, c_k, ϕ_k, ω_k are annual amplitude, phase and frequency, respectively, $k = 1$ is for the annual variation and $k = 2$ is for the semi-annual variation, and $\varepsilon(t)$ is the un-modeled residual term. The annual, semi-annual and secular terms in ice mass storage variations are then estimated.

3.1. Secular variations of glaciers

The trend of glacier mass variations from 10 years of monthly GRACE measurements (January 2003–December 2012) is obtained. Fig. 2 shows the trend of ice mass variations in the Tien Shan and surroundings. Most trends are negative, indicating that most of the glaciers are melting, particularly in the north and central Tien Shan. Here the four regions marked A, B, C and D are analyzed in details. The trends are -8.0 ± 0.39 mm/a in Region A, -1.0 ± 0.24 mm/a in Region B, -2.3 ± 0.26 mm/a in Region C and -0.2 ± 0.14 mm/a in Region D. The bottom left corner in Fig. 2 shows the glacier trend for the Pamirs, which is not discussed in this paper.

3.2. Seasonal variations

Fig. 3 shows annual amplitude and phase of ice mass variations in the Tien Shan, where the color value shows the annual amplitude in mm and the contour value denotes the phase of maximum ice mass. Ice mass storage in the Tien Shan is maximal in April-May, and the minimum is in November-December (Fig. 3). Fig. 4 shows annual cycle in

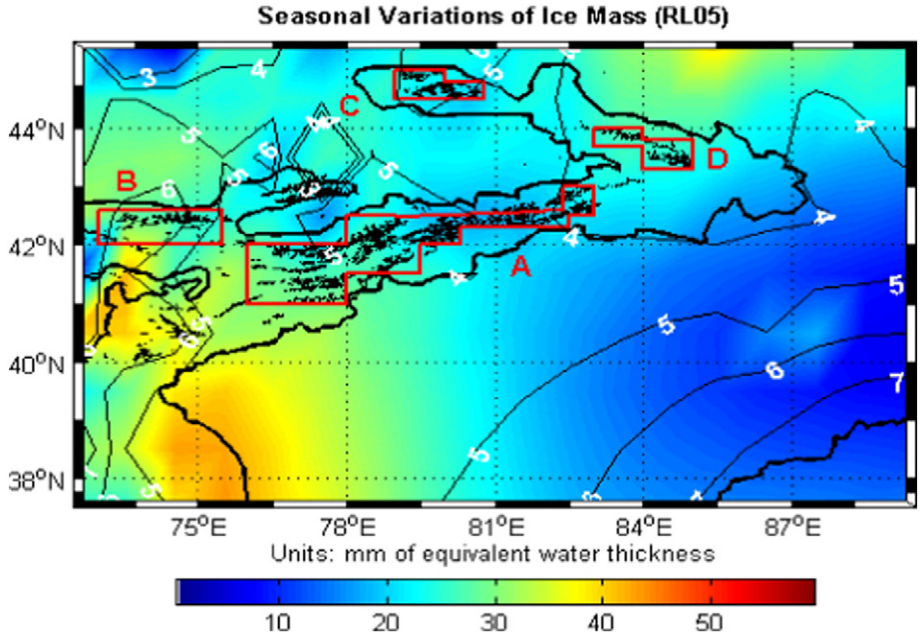

Fig. 3. Annual amplitude and phase of ice mass variations in the Tien Shan. The color value shows the annual amplitude in mm and the contour value denotes the phase of maximum ice mass. (For interpretation of the references to color in this figure legend, the reader is referred to the web version of this article.)

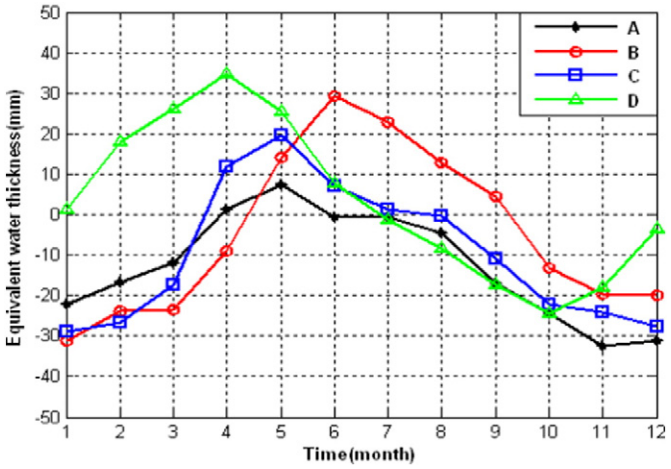

Fig. 4. Annual cycle of ice mass variations in the four regions of the Tien Shan.

Table 1
Annual amplitude and phase of ice mass variations in the four regions of the Tien Shan.

Region	Annual amplitude (mm)	Annual phase (°)	Month
A	17.62 ± 0.64	−61.15 ± 2.04	May
B	28.60 ± 0.56	−96.96 ± 2.59	June
C	21.59 ± 0.44	−73.66 ± 1.16	May
D	26.48 ± 0.25	−21.76 ± 0.73	April

four regions, A, B, C and D. The annual amplitude of the ice mass variability is 17.62 ± 0.64 mm in Region A, 28.60 ± 0.56 mm in Region B, 21.59 ± 0.44 mm in Region C and 26.48 ± 0.25 mm in Region D, and reaches its maximum in May in Region A, June in Region B, May in Region C and April in Region D (Table 1). Variability is similar in Regions A and C in annual amplitude (4 mm difference) and annual phase (12.5° difference). The annual amplitude for all regions is less than 30 mm and the largest is 28.60 mm in Region B. The seasonal variations are very weak in terms of snow from the WGHM model. The snow influence is reduced from the WGHM model, while the glacial ice still has the annual variations in mass.

3.3. Interannual variations

Fig. 5 shows the ice mass variability time series over the period from January 2003 to December 2012 based on GRACE and the WGHM model in the four different regions of the Tien Shan. The ice mass time series have significant interannual variability in the four regions. From 2003 to 2005, the trends in the four regions (A, B, C and D) are all positive, and the largest value, 23.7 mm/a is in Region B and the smallest, 0.4 mm/a is in Region D, indicating that the Tien Shan ice mass was thickening from 2003 to 2005. However, after 2005 the trend is negative. From 2005 to 2012, the trend in all regions is negative, −15.8 mm/a in Region A, with the minimum negative trend of −0.1 mm/a in Region D. That is, the Tien Shan ice mass has been melting since 2005.

4. Discussions

In order to further understand the reason of glacier mass changes in the Tien Shan, we discuss the influence of air temperature, precipitation

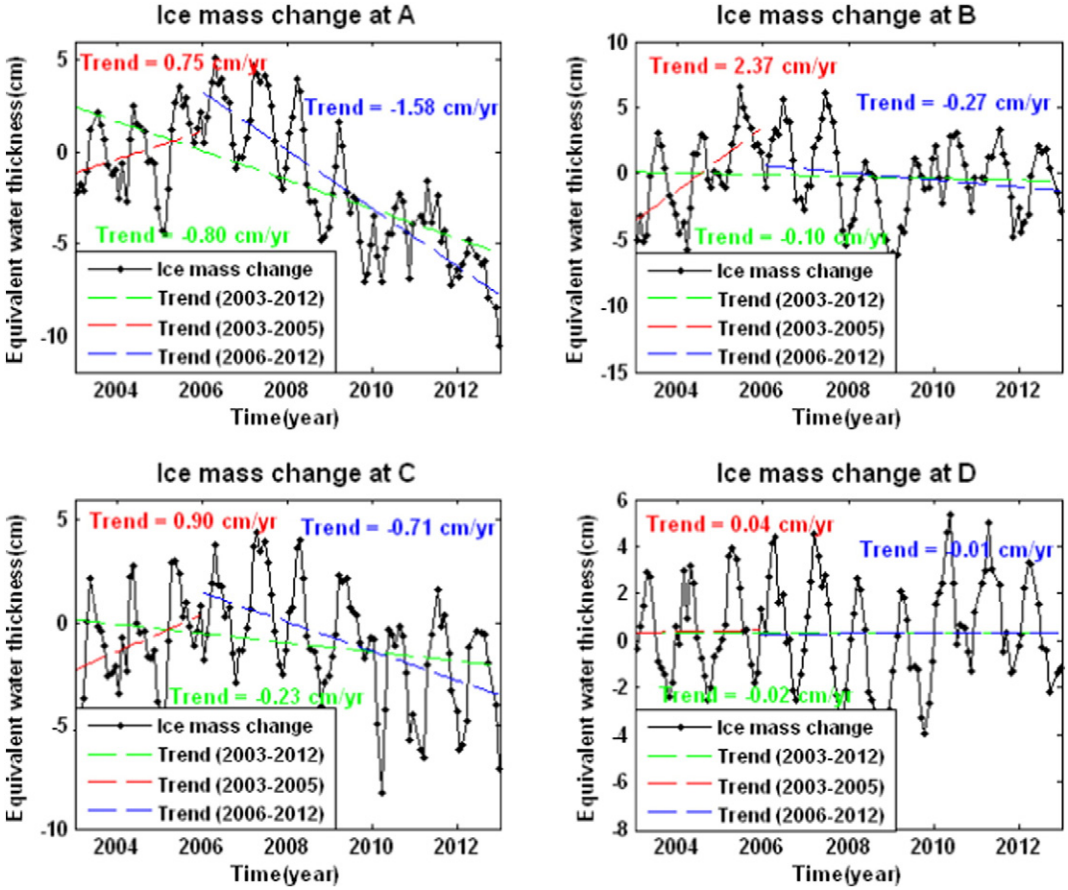

Fig. 5. Ice mass variability time series in Regions A to D of the Tien Shan.

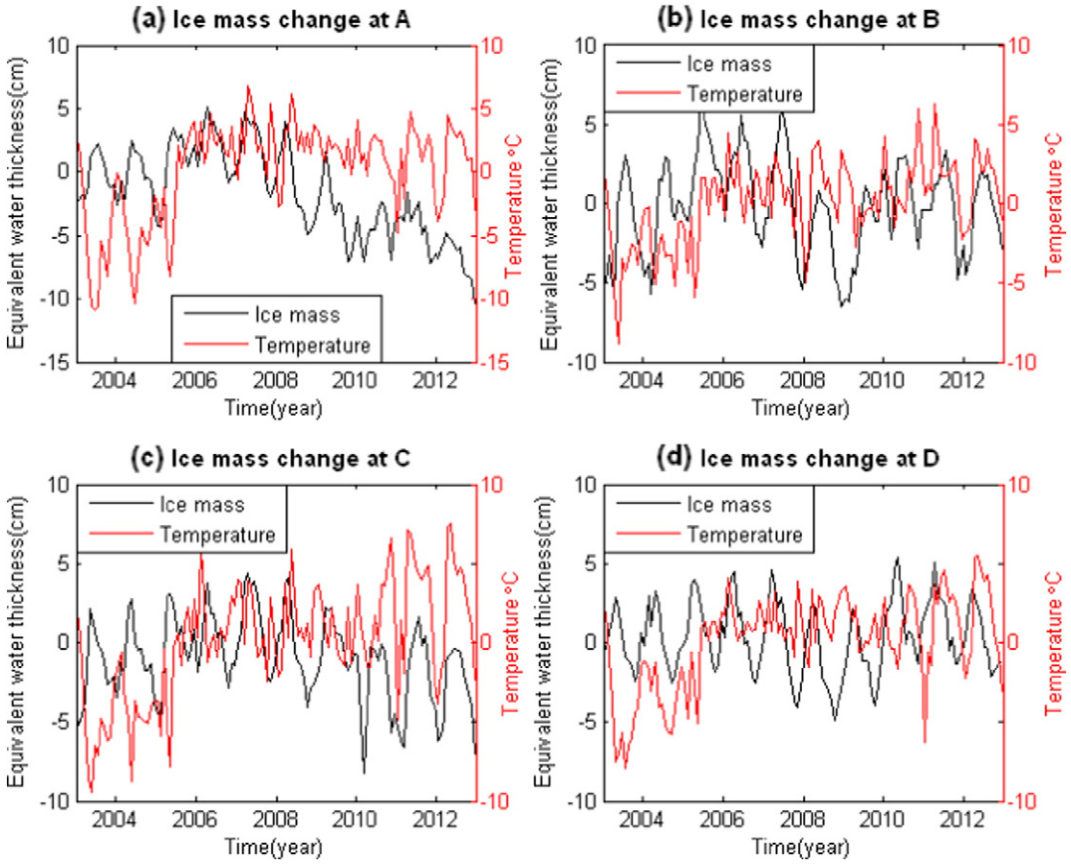

Fig. 6. Time series of glacier mass and air temperature changes in the four regions.

and evapotranspiration on the glacier mass balance (Changnon et al., 1988). Fig. 6 shows the time series of glacier mass change and air temperature change in Regions A to D. We see that over the past 10 years in all four regions, temperature has increased (seasonal variability has been removed in Fig. 6) by 0.66 °C/a in Region A, 0.49 °C/a in Region B, 0.78 °C/a in Region C and 0.57 °C/a in Region D. Before 2005, air temperature was clearly lower and then rapidly increases between 2005 and 2006, especially in Regions A, B and C. Air temperature has subsequently continued to increase from 2006 to 2012. The glacier changes are consistent with these air temperature changes in the four regions, and rising temperature is a direct cause of glacier recession in the Tien Shan over the period (e.g. Aizen et al., 2006).

Figs. 7, 8, 9 and 10 show the time series of glacier mass, precipitation and evapotranspiration in the four Regions A, B, C and D, respectively. The monthly precipitation data used in this study are derived from Global Precipitation Climatology Project database (GPCP). The GPCP quantifies the distribution of precipitation over the global land surface (Adler et al., 2003). The monthly evapotranspiration data are obtained from Global Land Data Assimilation System (GLDAS), which has been

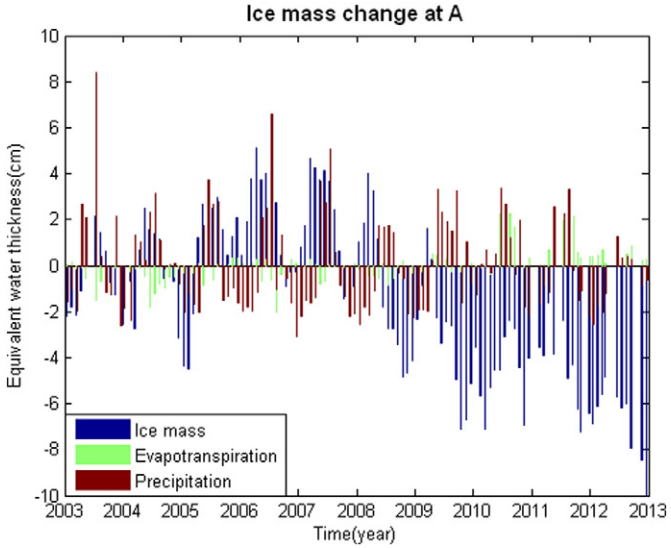

Fig. 7. Time series of glacier mass, precipitation and evapotranspiration in Region A.

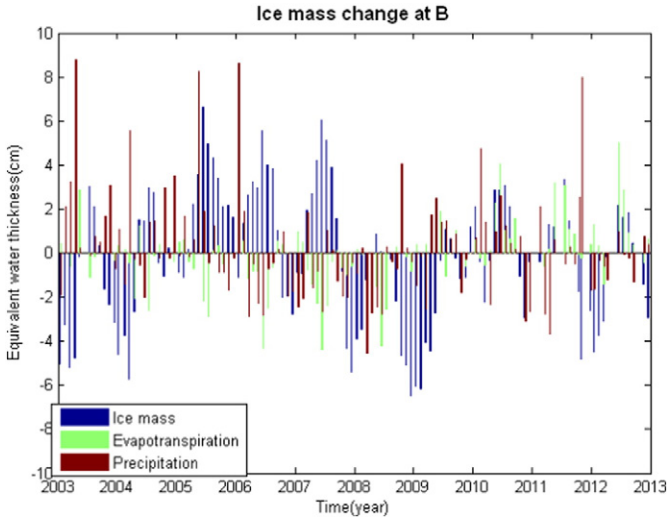

Fig. 8. Time series of glacier mass, precipitation and evapotranspiration in Region B.

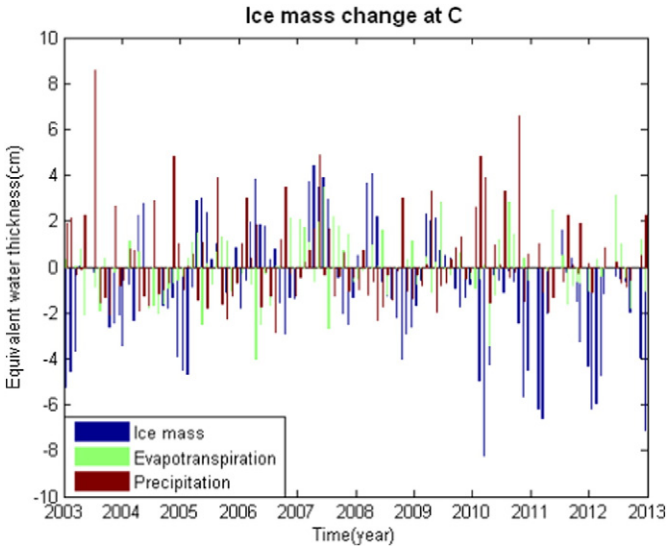

Fig. 9. Time series of glacier mass, precipitation and evapotranspiration in Region C.

jointly developed by the National Aeronautics and Space Administration (NASA) Goddard Space Flight Center (GSFC) and the National Oceanic and Atmospheric Administration (NOAA) National Centers for Environmental Prediction (NCEP) (Rodell et al., 2004). In order to compare with GRACE results, the averages from January 2003 to December 2012 are removed.

In Fig. 7, the glacial shrinkage in Region A seems associated with decreasing precipitation and increasing evapotranspiration. The secular trend is −0.64 mm/a in precipitation and 1.3 mm/a in evapotranspiration. Compared with precipitation and ice mass changes, the evapotranspiration is much smaller in Region A. The correlation coefficient is 0.39 between ice mass and precipitation change in Region A, while the ice mass and evapotranspiration changes are not strongly correlated. Thus, precipitation is an important factor in contributing to the glacial mass change in Region A. From Fig. 8, the secular trend is −2.03 mm/a in precipitation and 1.5 mm/a in evapotranspiration in Region B. The correlation coefficient is 0.34 between ice mass change and precipitation change, and 0.30 between ice mass change and evapotranspiration change. Since TWS is total ice mass variation as the integration of precipitation, evapotranspiration and runoff, namely:

$$dTWS/dt = P - ET - R \quad (3)$$

where P is the precipitation, ET is the evapotranspiration and R is the runoff. Neglecting R, the derivative of TWS is related to $(P - ET)$. The correction is above 0.5 between ice mass variation and $P - ET$, particularly in Region B. Thus, precipitation and evapotranspiration have joint effects on ice mass shrinkage in the Tian Shan.

From Fig. 9, changes in precipitation in Region C are not as significant as those of Regions A and B, but still show decreasing trends. The trend in precipitation is −0.06 mm/a and the trend in evapotranspiration is 0.48 mm/a. The correlation coefficient is 0.35 between ice mass change and evapotranspiration change, while ice mass change and precipitation change have weak correlation in Region C. In Region C therefore, evapotranspiration change has a more significant impact on glacier mass change than precipitation change. In Fig. 10, the variability in evapotranspiration is much smaller than the ice mass change and precipitation change. The trend in evapotranspiration is almost zero, while the trend in precipitation is −0.47 mm/a. Glacial shrinkage is therefore mainly related to decreasing precipitation in Region D.

In addition, the total land water storage is calculated from the WGHM model, including snow water storage, soil moisture storage, surface water storage and groundwater storage, while the WGHM model may not represent these components well. Furthermore, Glacial Isostatic Adjustment (GIA) also affects the glacier mass loss estimations, which should be considered in the future.

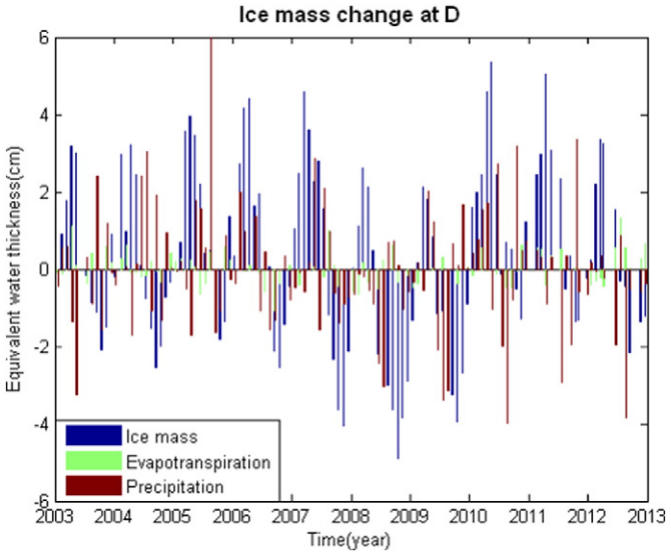

Fig. 10. Time series of glacier mass, precipitation and evapotranspiration in Region D.

5. Conclusions

In this paper, the seasonal, secular and interannual variations of over 10-year monthly ice mass in the Tien Shan are investigated from GRACE and the WGHM model. The annual amplitude of the ice mass variations is 17.62 mm in Region A, 28.60 mm in Region B, 21.59 mm in Region C and 26.48 mm in Region D. The annual ice mass storage reaches its maximum in April–June and minimum in November–December. Most glaciers in the Tian Shan are significantly melting. The trend of ice mass variability is −8.0 mm/a in Region A, −1.0 mm/a Region B, −2.3 mm/a Region C and −0.2 mm/a Region D. The trends in all four regions (A, B, C and D) were positive from 2002 to 2005 and negative from 2005 to 2012, indicating that the Tien Shan glaciers were increasing prior to 2005 and significantly melting since 2005.

The glacier variations are consistent with temperature changes in the four regions. Air temperature has increased in the past 10 years continuously, with a rapid increase between 2005 and 2006, especially in Regions A and B. Therefore, the rising temperature is the direct cause of glacier recession over the same period. In addition, in the past decade the precipitation has decreased and evapotranspiration has increased, also contributing to glacier melting. The influence of precipitation and evapotranspiration is different in different regions, but in Regions A and D, the precipitation has large effects on glacial changes.

Acknowledgments

We thank the Center for Space Research, University of Texas at Austin for providing the GRACE solutions. This research is supported by the Shanghai Science and Technology Commission Project (Grant No. 12DZ2273300), Key Laboratory of Planetary Sciences, Chinese Academy of Sciences and National Natural Science Foundation of China (NSFC) Project (Grant Nos. 11373059 and 11573052).

References

Adler, R.F., Huffman, G.J., Chang, A., 2003. Theversion-2 global precipitation climatology project (GPCP) monthly precipitation analysis (1979-present). J. Hydrometeorol. 4 (6), 1147–1167.

Aizen, V.B., Kuzmichenok, V.A., Surazakov, A.B., Aizen, E.M., 2006. Glacier changes in the central and northern Tien Shan during the last 140 years based on surface and remote-sensing data. Ann. Glaciol. 43, 202–213.
Avsar, N., Jin, S.G., Kutoglu, H., Gurbuz, G., 2016. Sea level change along the Black Sea coast from Satellite Altimetry, Tide Gauge and GPS observations. Geod. Geodyn. 7 (1), 50–55. http://dx.doi.org/10.1016/j.geog.2016.03.005.
Bettadpur, S., 2007. Level-2 Gravity Field Product User Handbook, GRACE 327–734, The GRACE Project. Cent. for Space Res., Univ. of Texas at Austin, Austin.
Changnon, S.A., Huff, F.A., Hsu, C.F., 1988. Relations between precipitation and shallow ground water in Illinois. J. Clim. 1, 1239–1250.
Cheng, M., Tapley, B.D., 2004. Variations in the Earth's oblateness during the past 28 years. J. Geophys. Res. 109, B09402. http://dx.doi.org/10.1029/2004JB003028.
Döll, P., Kaspar, F., Lehner, B., 2003. A global hydrological model for deriving water availability indicators: model tuning and validation. J. Hydrol. 270 (1–2), 105–134.
Frappart, F., Papa, F., Famiglietti, J.S., et al., 2008. Interannual variations of river water storage from a multiple satellite approach: a case study for the Rio Negro River basin. J. Geophys. Res. 113, D21104. http://dx.doi.org/10.1029/2007JD009438.
Geruo, A., Wahr, J., Zhong, S., 2013. Computations of the viscoelastic response of a 3-D compressible Earth to surface loading: an application to Glacial Isostatic Adjustment in Antarctica and Canada. Geophys. J. Int. 192, 557–572. http://dx.doi.org/10.1093/gji/ggs030.
Güntner, A., Stuck, J., Werth, S., Döll, P., Verzano, K., Merz, B., 2007. A global analysis of temporal and spatial variations in continental water storage. Water Resour. Res. 43, W05416. http://dx.doi.org/10.1029/2006WR005247.
Han, D., Wahr, J., 1995. The viscoelastic relaxation of a realistically stratified earth, and a further analysis of post-glacial rebound. Geophys. J. Int. 120 (2), 287–311. http://dx.doi.org/10.1111/j.1365-246X.1995.tb01819.x.
Hassan, A., Jin, S.G., 2016. Water storage changes and balances in Africa observed by satellite gravimetry and hydrologic models. Geod. Geodyn. 7 (1), 39–49. http://dx.doi.org/10.1016/j.geog.2016.03.002.
Jekeli, C., 1981. Alternative methods to smooth the Earth's gravity field. Rep.327, D. Sci. & Surv.Ohio State University, Columbus, OH
Jin, S.G., Feng, G.P., 2013. Large-scale variations of global groundwater from satellite gravimetry and hydrological models, 2002–2012. Glob. Planet. Change 106, 20–30. http://dx.doi.org/10.1016/j.gloplacha.2013.02.008.
Jin, S.G., Chambers, D., Tapley, B., 2010. Hydrological and oceanic effects on polar motion from GRACE and models. J. Geophys. Res. 115, B02403. http://dx.doi.org/10.1029/2009JB006635.
Jin, S.G., Zhang, L., Tapley, B., 2011. The understanding of length-of-day variations from satellite gravity and laser ranging measurements. Geophys. J. Int. 184 (2), 651–660. http://dx.doi.org/10.1111/j.1365-246X.2010.04869.x.
Jin, S.G., Hassan, A., Feng, G., 2012. Assessment of terrestrial water contributions to polar motion from GRACE and hydrological models. J. Geodyn. 62, 40–48. http://dx.doi.org/10.1016/j.jog.2012.01.009.
Jin, S.G., van Dam, T., Wdowinski, S., 2013. Observing and understanding the Earth system variations from space geodesy. J. Geodyn. 72, 1–10. http://dx.doi.org/10.1016/j.jog.2013.08.001.
Jin, S.G., Feng, G.P., Anderson, O., 2014. Errors of mean dynamic topography and geostrophic currents estimates in China's Marginal Sea from GOCE and satellite altimetry. J. Atmos. Ocean. Technol. 31 (11), 2544–2555. http://dx.doi.org/10.1175/JTECH-D-13-00243.1.
Jing, Z., Jiao, K., Yao, T., Wang, N., Li, Z., 2006. Mass balance and recession of Urumqi glacier No. 1, Tien Shan, China, over the last 45 years. Ann. Glaciol. 43, 214–217.
Landerer, F.W., Swenson, S.C., 2012. Accuracy of scaled GRACE terrestrial water storage estimates. Water Resour. Res. 48, W04531. http://dx.doi.org/10.1029/2011WR011453.
Li, B., Zhu, A.X., Zhang, Y., Pei, T., Qin, C., Zhou, C., 2006. Glacier change over the past four decades in the middle Chinese Tien Shan. J. Glaciol. 52 (178), 425–432.
Liu, S., Ding, Y., Shangguan, D., Zhang, Y., Li, J., Han, H., Wang, J., Xie, C., 2006. Glacier retreat as a result of climate warming and increased precipitation in the Tarim River basin, Northwest China. Ann. Glaciol. 43, 91–96.
Morison, J., Wahr, J., Kwok, R., et al., 2007. Recent trends in Arctic Ocean mass distribution revealed by GRACE. Geophys. Res. Lett. 34, L07602. http://dx.doi.org/10.1029/2006GL029016.
Narama, C., Shimamura, Y., Nakayama, D., Abdrakhmatov, K., 2006. Recent changes of glacier coverage in the western Terskey–Alatoo range, Kyrgyz Republic, using Corona and Landsat. Ann. Glaciol. 43, 223–229.
Niederer, P., Bilenko, V., Ershova, N., Hurni, H., Yerokhin, S., Maselli, D., 2008. Tracing glacier wastage in the Northern Tien Shan (Kyrgyzstan/Central Asia) over the last 40 years. Clim. Chang. 86 (1–2), 227–234.
Paulson, A., Zhong, S., Wahr, J., 2007. Inference of mantle viscosity from GRACE and relative sea level data. Geophys. J. Int. 171, 497–508. http://dx.doi.org/10.1111/j.1365-246X.2007.03556.x.
Rodell, M., Houser, P.R., Jambor, U., et al., 2004. The global land data assimilation system. Bull. Am. Meteorol. Soc. 85 (3), 381–394. http://dx.doi.org/10.1175/BAMS-85-3-381.
Rodell, M., Velicogna, I., Famiglietti, J.S., 2009. Satellite-based estimates of groundwater depletion in India. Nature 460, 999–1002. http://dx.doi.org/10.1038/nature08238.
Shangguan, D., Liu, S., Ding, Y., Ding, L., Xiong, L., Cai, D., Li, G., Lu, A., Zhang, S., Zhang, Y., 2006. Monitoring the glacier changes in the Muztag Ata and Konggur mountains, east Pamirs, based on Chinese Glacier Inventory and recent satellite imagery. Ann. Glaciol. 43, 79–85.
Shen, C., Xuan, S., Zou, Z., Wu, G., 2015. Trends in gravity changes from 2009 to 2013 derived from ground-based gravimetry and GRACE data in North China. Geod. Geodyn. 6 (6), 423–428. http://dx.doi.org/10.1016/j.geog.2015.08.001.
Swenson, S.C., Wahr, J., 2002. Methods for inferring regional surface-mass anomalies from Gravity Recovery and Climate Experiment (GRACE) measurements of time-variable gravity. J. Geophys. Res. 107 (B9), 2193. http://dx.doi.org/10.1029/2001JB000576.
Swenson, S.C., Wahr, J., 2006. Post-processing removal of correlated errors in GRACE data. Geophys. Res. Lett. 33, L08402. http://dx.doi.org/10.1029/2005GL025285.
Swenson, S., Chambers, D., Wahr, J., 2008. Estimating geocenter variations from a combination of GRACE and ocean model output. J. Geophys. Res. 113, B08410. http://dx.doi.org/10.1029/2007JB005338.
Velicogna, I., 2009. Increasing rates of ice mass loss from the Greenland and Antarctic ice sheets revealed by GRACE. Geophys. Res. Lett. 36, L19503. http://dx.doi.org/10.1029/2009GL040222.
Velicogna, I., Wahr, J., 2005. Greenland mass balance from GRACE. Geophys. Res. Lett. 32, L18505. http://dx.doi.org/10.1029/2005GL023955.
Wahr, J., Molenaar, M., Bryan, F., 1998. Time-variability of the Earth's gravity field: hydrological and oceanic effects and their possible detection using GRACE. J. Geophys. Res. 103, 30205–30229.
Zhao, Q., Wu, W., Wu, Y., 2015. Variations in China's terrestrial water storage over the past decade using GRACE data. Geod. Geodyn. 6 (3), 187–193. http://dx.doi.org/10.1016/j.geog.2015.03.004.